Biomaterials Advances 160 (2024) 213840

Contents lists available at ScienceDirect

Biomaterials Advances

journal homepage: www.journals.elsevier.com/materials-science-and-engineering-c

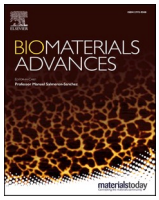

Remarkable enhancement of cinnamaldehyde antimicrobial activity encapsulated in capped mesoporous nanoparticles: A new "nanokiller" approach in the era of antimicrobial resistance

Ángela Morellá-Aucejo [a,b,e], Serena Medaglia [a,b], María Ruiz-Rico [c], Ramón Martínez-Máñez [a,b,d,e,f], María Dolores Marcos [a,b,e,f,*], Andrea Bernardos [a,b,e,f,*]

[a] Instituto Interuniversitario de Investigación de Reconocimiento Molecular y Desarrollo Tecnológico (IDM), Universitat Politècnica de València and Universitat de València, Camino de Vera s/n, 46022 Valencia, Spain
[b] CIBER de Bioingeniería, Biomateriales y Nanomedicina (CIBER-BBN), Instituto de Salud Carlos III, 46022 Valencia, Spain
[c] Instituto Universitario de Ingeniería de Alimentos (FoodUPV), Universitat Politècnica de València, Camino de Vera s/n, 46022 Valencia, Spain
[d] Unidad Mixta de Investigación en Nanomedicina y Sensores, Universitat Politècnica de València, Instituto de Investigación Sanitaria La Fe (IISLAFE), Av Fernando Abril Martorell 106, 46026 Valencia, Spain
[e] Unidad Mixta UPV-CIPF de Investigación en Mecanismos Enfermedades y Nanomedicina, Universitat Politècnica de València, Centro de Investigación Príncipe Felipe, C/Eduardo Primo Yúfera 3, 46012 Valencia, Spain
[f] Departamento de Química, Universitat Politècnica de València, Camino de Vera s/n, 46022 Valencia, Spain

ARTICLE INFO

Keywords:
Gated-nanodevice
Cinnamaldehyde
Pathogenic microorganisms
Antimicrobial resistance

ABSTRACT

Combating antimicrobial resistance is one of the biggest health challenges because of the ineffectiveness of standard biocide treatments. This challenge could be approached using natural products, which have demonstrated powerful therapeutics against multidrug-resistant microbes. In the present work, a nanodevice consisting of mesoporous silica nanoparticles loaded with an essential oil component (cinnamaldehyde) and functionalized with the polypeptide ε-poly-L-lysine is developed and used as an antimicrobial agent. In the presence of the corresponding stimuli (i.e., exogenous proteolytic enzymes from bacteria or fungi), the polypeptide is hydrolyzed, and the cinnamaldehyde delivery is enhanced. The nanodevice's release mechanism and efficacy are evaluated in vitro against the pathogenic microorganisms *Escherichia coli*, *Staphylococcus aureus*, and *Candida albicans*. The results demonstrate that the new device increases the delivery of the cinnamaldehyde via a biocontrolled uncapping mechanism triggered by proteolytic enzymes. Moreover, the nanodevice notably improves the antimicrobial efficacy of cinnamaldehyde when compared to the free compound, ca. 52-fold for *E. coli*, ca. 60-fold for *S. aureus*, and ca. 7-fold for *C. albicans*. The enhancement of the antimicrobial activity of the essential oil component is attributed to the decrease of its volatility due to its encapsulation in the porous silica matrix and the increase of its local concentration when released due to the presence of microorganisms.

1. Introduction

During the last years, the indiscriminate and inappropriate use of drugs and phytosanitary products has often produced the inefficacy of common antimicrobial treatments. One of the biggest challenges in today's health is to prevent and combat the so-called antimicrobial resistance (AMR). AMR occurs when bacteria, fungi, viruses, and parasites do not respond to antimicrobial therapy, and the treatment of infections derived from them is complicated, increasing the risk of disease spread, lethality, and the cost of treatment [1]. In this context, it is necessary to develop new antimicrobial products for their application in medicine and the agri-food sector to avoid antimicrobial resistance. In this scenario, naturally occurring antimicrobial compounds are an excellent proposal as alternative antimicrobial agents [2]. Antimicrobial compounds of natural origin can be obtained from plants, animals, or microorganisms. Examples of natural antimicrobials are essential oil components (EOCs), i.e., bioactive compounds from lipophilic plant extracts [3], that can be extracted from roots, leaves, seeds or flowers.

* Corresponding authors at: Instituto Interuniversitario de Investigación de Reconocimiento Molecular y Desarrollo Tecnológico (IDM), Universitat Politècnica de València and Universitat de València, Camino de Vera s/n, 46022 Valencia, Spain.
E-mail address: anberba@upvnet.upv.es (A. Bernardos).

https://doi.org/10.1016/j.bioadv.2024.213840
Received 14 September 2023; Received in revised form 8 March 2024; Accepted 23 March 2024
Available online 26 March 2024

EOCs present recognized antioxidant, antibacterial, antifungal, and insecticidal properties [4] and are considered biodegradable and less toxic than synthetic antimicrobials. These EOCs are produced as a defensive mechanism by the plant. When in contact with microorganisms, they create a series of cascade reactions that ultimately disrupt the bacterial or fungal cell, making them effective for the inactivation or inhibition of many microorganisms [5,6]. Moreover, the multicomponent nature of EOCs can reduce the potential AMR to essential oils [7], making EOCs excellent candidates for use as natural antimicrobials. Besides, it has been reported that EOCs can avoid AMR thanks to their action mechanism related to protein biosynthesis and alteration of cell walls and membranes [8].

Extensive research has been conducted on various medical applications related to EOCs. These include its anticancer and antitumor properties, cardioprotective function, anti-inflammatory properties, thermogenic effects, and antimicrobial properties [9]. However, EOCs have technological drawbacks such as high volatility, strong sensorial properties, high reactivity, and poor water solubility, which need to be addressed before their application in a real scenario [10]. Research in recent years has focused on developing technologies, such as nanoencapsulation and nanoparticle incorporation, to solve these disadvantages [11,12]. These nanodevices can have different characteristics, such as organic or inorganic nature, or different sizes and shapes, which render them various properties for specific applications [13,14]. These nanodevices can release the cargo in two different ways: (i) passive, through a sustained release of the cargo, or (ii) on-command, in which the nanodevice delivers its cargo in the presence of a given stimulus [15,16].

Among different nanodevices, mesoporous silica nanoparticles (MSNs) have been used in recent years as potential drug delivery carriers for the protection and controlled release of several entrapped cargos [17–19]. One of the most valuable properties of MSNs is the possibility of designing innovative delivery systems by incorporating molecular gates (also known as gatekeepers) into the siliceous carrier. The molecular gate is usually anchored on the surface of the porous silica nanoparticles and prevents cargo delivery until a suitable stimulus triggers cargo release. Recently, controlled release using gated materials has been an emerging and innovative concept that has been applied in drug delivery [20,21], sensing [22,23], chemical communication [24,25], and in antimicrobial applications [11,26], among others. In the area of biomedicine and agri-food, several molecular gates have recently been developed, including pH-responsive [27,28], saccharide-responsive [29,30], and polymeric or protein-containing gates [11,31]. One example of a protein that can act as a gatekeeper is ε-poly-L-lysine (EPL), a natural hydrophilic cationic linear antimicrobial peptide composed of 25 to 35 identical L-lysine units (3500–4000 Da) that has been used as a safe and natural food preservative, and it is approved by US Food and Drug Administration (FDA), due to its antimicrobial efficacy [32,33], non-toxic properties, even at high doses, and biodegradability by amidases and proteases [34,31,36]. Although previous studies indicate that the antibacterial capacity of the EPL in solution does not have any particular behavior in response to pH, it has been shown that the most suitable pH range for its antimicrobial activity is close to physiological pH (between 6.0 and 8.0) for free EPL and EPL composites [37]. All these properties make EPL a desirable option for preparing new ecological and environmentally friendly antimicrobial compounds [38].

In this scenario, we report herein the design and application of an antimicrobial gated nanodevice against pathogenic microorganisms based on MSNs loaded with the EOC cinnamaldehyde and covalently functionalized with EPL. The designed nanodevice responds to the presence of bacterial and yeast protease secretion [39–41], which allows the improvement of the release of the entrapped EOC that exerts an inhibitory effect on microorganisms. To the best of the authors' knowledge, no examples of biocidal nanodevices based on natural antimicrobials effective at concentrations as low as those presented in this work have been developed.

2. Materials and methods

2.1. Chemicals

Tetraethyl orthosilicate (TEOS), *n*-cetyltrimethylammonium bromide (CTABr), sodium hydroxide (NaOH), trans-cinnamaldehyde (Cin), pronase from *Streptomyces griseus*, 3-(triethoxysilyl)propyl isocyanate (NCO) and triethylamine (TEA) were provided by Sigma-Aldrich (Madrid, Spain). Mueller Hinton Broth (MHB), Mueller Hinton Agar (MHA), Ringer ¼ powder, hexane, and acetonitrile (ACN) were provided by Scharlab (Barcelona, Spain). Poly-epsilon-L-lysine hydrochloride was provided by Carbosynth (Bratislava, Slovakia). Buffered peptone water was purchased from Liofilchem (Roseto degli Abruzzi, Italy). Yeast extract peptone dextrose (YPD) was supplied by MP Biomedicals (Eschwege, Germany). Agar powder, SM plate count agar, and tween 80 were purchased from Himedia (Einhausen, Germany). LIVE/DEAD BacLight Bacterial Viability Kit and LIVE/DEAD Yeast Viability Kit were provided from Invitrogen, ThermoFisher Scientific (Madrid, Spain).

2.2. Microorganism strains and culture conditions

The following strains were used as model microorganisms to evaluate the antimicrobial properties of the nanodevice: the Gram-negative bacterium *Escherichia coli* (*E. coli*), the Gram-positive bacterium *Staphylococcus aureus* (*S. aureus*), and the yeast *Candida albicans* (*C. albicans*). The *E. coli* (CECT 433) strain used in this study was obtained from the Spanish Type Culture Collection (CECT, Burjassot, Spain). The *S. aureus* (ATCC 25923) strain used in this study was obtained from the American Type Culture Collection (ATCC, Virginia, USA). Standard methods for bacteria culture and manipulation were used. *E. coli* was grown in peptone water broth (PWB) at 37 °C for 24 h and plated in plate count agar (PCA). *S. aureus* was grown in Mueller-Hinton broth (MHB) at 37 °C for 24 h to achieve a stationary phase and plated in Mueller-Hinton agar (MHA). The *C. albicans* (CECT 1002T) yeast strain used in this study was obtained from the Spanish Type Culture Collection (CECT, Burjassot, Spain). Standard methods for yeast culture and manipulation were used. *C. albicans* was grown in yeast peptone dextrose broth (YPD) at 26 °C 24 h to achieve a stationary phase and plated in yeast peptone dextrose agar (YPDA).

2.3. Synthesis of mesoporous silica nanoparticles (MSN_{cal})

Briefly, 1 g (2.74 mmol) of *n*-cetyltrimethylammonium bromide (CTABr) was dissolved in 480 mL of deionized water using magnetic stirring. Next, 3.5 mL of a 2 mol·L^{-1} NaOH solution was added, and the temperature was increased to 80 °C. Then, the silica precursor, tetraethyl orthosilicate (TEOS) (5 mL, 22.4 mmol), was added dropwise into the solution. Magnetic stirring and temperature were kept for 2 h to obtain a white suspension. Finally, the solid was isolated by filtration, washed several times with plenty of water until neutral pH, and dried at 80 °C overnight (**MSN_{asmade}**). Subsequently, the calcination procedure was performed at 550 °C in an oxidant atmosphere for 5 h to remove CTABr and obtain the final mesoporous silica nanoparticles (**MSN_{cal}**).

2.4. Synthesis of $MSN_{EPL\text{-}Cin}$

Firstly, to obtain the nanodevice **$MSN_{EPL\text{-}Cin}$**, a cargo loading process was performed by steam adsorption. For that, 100 mg of MSNs and 100 mg of cinnamaldehyde were mixed in a perfectly closed vial, and the mixtures were shaken at 40 °C for 24 h to achieve the loading of the pores. When the loading procedure finished, the solid looked completely dry because of the complete absorption of the EOC. This gives the solid **MSN_{Cin}**. Then, to functionalize the surface with isocyanate moieties, an excess of 3-(triethoxysilyl)propylisocyanate (NCO) (200 mL, 4.25

mmol·g^{-1} solid) was added to a suspension of 200 mg of **MSN$_{Cin}$** in 6 mL of ACN and the mixture was stirred for 5.5 h. The solid was isolated by filtration and dried under vacuum (**MSN$_{NCO\text{-}Cin}$**). For coating MSNs, EPL (200 mg, 0.05 mmol, 0.25 mmol of polymer·g^{-1} solid) was dissolved in 4.5 mL of deionized water. Next, 9 mL of ACN and 200 mg of **MSN$_{NCO\text{-}Cin}$** were incorporated into the EPL solution. 300 mL of triethylamine was added to improve the urea bond formation, and the mixture was stirred for 3 h. Finally, the nanodevice (**MSN$_{EPL\text{-}Cin}$**) was isolated by centrifugation, washed thoroughly with deionized water, dried under vacuum, and stored at 4 °C until use.

2.5. Synthesis of MSN_{EPL}

A solid without loaded cinnamaldehyde but gated with the EPL was also synthesized, following the procedure described in Section 2.4. In this case, the functionalization of the surface with isocyanate moieties was performed using (**MSN$_{cal}$**) as the starting material to obtain **MSN$_{NCO}$**, which was further coated with EPL, resulting in the solid **MSN$_{EPL}$**.

2.6. Materials characterization

Transmission electron microscopy (TEM), N_2 adsorption-desorption isotherms, powder X-ray diffraction (PXRD), TEM coupled with energy dispersive X-ray spectroscopy (TEM-EDX), thermogravimetric analysis (TGA), ζ potential, dynamic light scattering (DLS), infrared spectroscopy (FTIR), UV–visible spectrophotometry, and confocal microscopy techniques were employed for materials characterization. TEM images were acquired using a JEOL JEM 1400F Electron microscope (JEOL Europe SAS, Croissysur-Seine, France) working at 120 kV. N_2 adsorption-desorption isotherms were obtained using a Micromeritics TriStar II Plus automated analyzer (Micromeritics Instrument Corporation, Norcross, USA). Samples were previously degassed at 90 °C in vacuum overnight, and measurements were performed at 77 K. PXRD measurements were recorded on a Bruker D8 Advance diffractometer (Bruker, Coventry, UK) using CuKα radiation at low angles ($1.3 < 2\theta < 8.3$, with steps of 0.04 degrees and 3 s for step). TEM-EDX was also employed for element mapping using a JEOL TEM-2100F microscope. TGA determinations were performed in TGA/SDTA 851e Mettler Toledo balance (Mettler Toledo Inc., Schwarzenbach, Switzerland) in an oxidant atmosphere (air, 80 mL/min) with a heating program that consisted of a heating ramp of 10 °C/min from 393 K to 1273 K, and an isothermal heating step at this temperature for 30 min. ζ potential studies were carried out using a ZetaSizer Nano ZS (Malvern Instruments, UK), and DLS studies were performed using a Nanosight NS300 (Malvern Panalytical, Spain). The corresponding materials were suspended in distilled water at a concentration of 1 mg mL^{-1} to carry out the experiments. FT-IR spectra were obtained in a Bruker Tensor 27 FTIR spectrometer (Bruker, Coventry, UK). UV–visible spectra were recorded with a JASCO V-630 Spectrophotometer (Jasco Analitica, Spain). Confocal microscopy imaging was performed employing a Leica TCS SPE (Leica Microsystems Heidelberg GmbH, Germany) inverted laser scanning confocal microscope using an HC PL APO 100× oil objective and an HC PL APO 63× oil objective.

2.7. Cinnamaldehyde payload quantification

An extraction with hexane was performed to determine the payload content in **MSN$_{EPL\text{-}Cin}$**. For this purpose, 1 mg of **MSN$_{EPL\text{-}Cin}$** was suspended in 1 mL of hexane, and the mixture was kept under stirring for 24 h. Then, the sample was centrifuged to remove the solid, and the released Cin payload was quantified with a calibration curve measuring the absorbance of the supernatant at 280 nm.

2.8. Responsive delivery studies of cinnamaldehyde

Release assays confirmed the ability of the EPL protein to regulate Cin payload delivery from **MSN$_{EPL\text{-}Cin}$** and quantify the cargo release. 3 mg of **MSN$_{EPL\text{-}Cin}$** were suspended in 1 mL in the absence (blank) or the presence of protease enzyme from *Streptomyces griseus* (1 mg·mL^{-1}). The solutions were kept under stirring at 37 °C. At certain times (0, 1, 3, 5, 24 h), aliquots (1 mL) were taken. Then, 0.5 mL of hexane was added to each aliquot, and the mixtures were shaken to extract the cinnamaldehyde from the aqueous phase. Organic phases were collected for cinnamaldehyde quantification. The extraction procedure was carried out three times in each aliquot. The cinnamaldehyde released was quantified by its absorbance band at 280 nm.

2.9. Antimicrobial susceptibility assays

According to the nanodevice design, the antimicrobial properties of the nanodevice would be based on the antimicrobial EOC entrapped in the pores of the support together with the antimicrobial peptide coated on the surface of the support. To determine the different elements' role in the nanodevice's antimicrobial properties, the antimicrobial susceptibility assays were performed in parallel with the solids **MSN$_{EPL\text{-}Cin}$**, **MSN$_{EPL}$**, and free EOC. Since bacteria and yeast normally cannot endocytose nanoparticles [42,43], as occurs in other cell types, the amount of cinnamaldehyde released from **MSN$_{EPL\text{-}Cin}$** due to degradation of the molecular gate (EPL) by the presence of proteases in the medium would be mainly responsible for the antimicrobial properties of the nanodevice. The amount of cinnamaldehyde released into the medium per mg of solid (see Section 2.9.2) was taken as the free equivalent for the antimicrobial assays.

2.9.1. Bactericidal and fungicidal activity of the nanodevice

S. aureus, *E. coli*, and *C. albicans* strains were grown following the conditions described in Section 2.2 to obtain the corresponding inoculum with a cellular density of approximately 1×10^9 CFU·mL^{-1}. The optical density (OD) of the culture was measured by UV–visible spectroscopy to estimate the growth of the cells, and they were diluted in Ringer solution to obtain inocula of 10^6 CFU·mL^{-1} for bacterial strains and 10^8 CFU·mL^{-1} for the yeast strain.

The antimicrobial activity of the nanodevices was determined by antimicrobial susceptibility assays. Different concentrations of **MSN$_{EPL\text{-}Cin}$** were prepared diluting from a suspension of 1250 μg·mL^{-1} of **MSN$_{EPL\text{-}Cin}$** in an isotonic diluent, Ringer solution, to obtain a range of final concentrations of 0, 2.44, 4.88, 9.77, 19.53, 39.06 and 78.13 μg·mL^{-1}.100 μL aliquot of each microorganism inoculum was added to each 900 μL solid suspension, obtaining a final concentration of microorganisms of 10^5 CFU·mL^{-1} for bacterial strains and 10^7 CFU mL^{-1} for yeast strain. Equivalent concentrations of free Cin were prepared to compare with the antimicrobial properties of free and encapsulated EOC. The samples were incubated with orbital stirring (280 rpm) at 37 °C for 24 h for the bacterial strains and at 26 °C for 24 h for the yeast strain.

After incubation, viable cell numbers were determined as colony-forming units (CFU) by spread plate technique. In triplicate, 20 μL of each sample was dropped by the Miles and Misra method [44] into a MHA for *S. aureus*, PCA for *E. coli*, and YPDA for *C. albicans* plates. After incubation at optimal temperatures for 24 h, the number of grown colonies was counted, and these values were logarithmically transformed and expressed as $\log_{10}$ CFU·mL^{-1}. The same procedure was performed to evaluate the antimicrobial properties of empty **MSN$_{EPL}$**. Positive (Ringer solution, Ringer solution with **MSN$_{cal}$** or Ringer solution with **MSN$_{NCO}$** inoculated) and negative controls (Ringer solution, Ringer solution with **MSN$_{cal}$** or Ringer solution with **MSN$_{NCO}$** non-inoculated) were included in all the assays. All the antimicrobial assays were tested in triplicate.

2.9.2. Microbial growth inhibition capacity of the nanodevice

The minimum inhibitory concentration (MIC) was obtained using the resazurin-based 96-well plate microdilution method [45,46]. Resazurin is a non-fluorescent (blue) dye that is reduced by active microbial cells to the fluorescent (pink) resorufin, giving a direct quantifiable measure of microbial metabolic activity [47]. Therefore, the MIC was defined as the lowest concentration of the nanodevice that inactivated the microbial cells, resulting in no dye reduction. Different **$MSN_{EPL\text{-}Cin}$** nanodevice concentrations were prepared diluting in a proper optimal nutritive broth medium, within a range of final concentration of 0, 2.44, 4.88, 9.77, 19.53, 39.06, 78.13, 156.25, 312.5 and 625 $\mu g \cdot mL^{-1}$ against the bacterial strains and 0, 19.53, 39.06, 78.13, 156.25, 312.5 625,1250, 2500, 5000 $\mu g \cdot mL^{-1}$ against the yeast strain. 100 μL microorganism inocula were added to each 100 μL solid suspension. Equivalent concentrations of free cinnamaldehyde were prepared to compare with the antimicrobial properties of free and encapsulated EOC within a range of final concentration of 0, 3.90, 7.81, 15.63, 31.25, 62.5, 125, 250, 500, and 1000 $\mu g \cdot mL^{-1}$.

Samples were incubated at 37 °C for 24 h for the bacterial strains and at 26 °C for 24 h for the yeast strain. After incubation, 30 μL of resazurin solution (0.015 %) was added to each sample, and the plate was incubated for 2 h at optimal conditions. Then, the microbial metabolic activity of the samples was established by visual detection of color change. The same procedure was performed to evaluate the antimicrobial properties of **MSN_{EPL}**. All the antimicrobial assays were tested in triplicate, including the same positive and negative controls described in Section 2.9.1.

The minimum bactericidal or fungicidal concentration (MBC or MFC) was determined by the microdilution method [45,46]. The MBC/MFC was defined as the lowest concentration of **$MSN_{EPL\text{-}Cin}$** that could kill 99.9 % of bacteria and yeast cells. The same concentration range of **$MSN_{EPL\text{-}Cin}$**, **MSN_{EPL}**, and free cinnamaldehyde and procedure were used as described above for the MIC assays. Following the incubation of samples, 20 μL of each sample was dropped by the Miles and Misra method [44] into an MHA for *S. aureus*, PCA for *E. coli*, and YPDA for *C. albicans* plates. After incubation at optimal temperatures for 24 h, the number of grown colonies was counted, and these values were logarithmically transformed and expressed as $\log_{10}$ $CFU \cdot mL^{-1}$.

2.9.3. Determination of microbial viability and agglomeration by fluorescence assay

In addition to plate count and metabolic activity techniques, the viability of the treated microorganisms was evaluated in terms of membrane cell integrity. The studied conditions included positive controls (non-treated microorganisms), microorganisms treated with 1/2 MIC and MIC of **$MSN_{EPL\text{-}Cin}$**, and microorganisms treated with the equivalent concentration of Cin released by **$MSN_{EPL\text{-}Cin}$** at the MIC dose, based on the MIC assays results.

The LIVE/DEAD BacLight™ bacterial viability kit (ThermoFisher Scientific, UK) was used to visualize the viable and dead bacterial cells according to the membrane cell integrity. This kit is composed of two fluorescent reagents: SYTO 9 (green-fluorescent nucleic acid stain), which marks all microbial cells with injured or intact membranes, and propidium iodide (red-fluorescent nucleic acid stain), which penetrates exclusively the microorganisms with damaged membranes, reducing SYTO 9 stain fluorescence when both are coexisting in the same cell. This results in a green/red labeling of the living/dead cells. The kit components were mixed at a ratio of 1:1, and 0.3 μL of the mixture was added to 100 μL of each microbial suspension. The suspension was mixed and incubated in the dark for 10 min to allow the penetration of dyes. Then, 10 μL of the stained cells were dropped on poly-L-lysine-covered slides (ThermoFisher Scientific, UK) and sealed with a coverslip. Finally, slides were visualized by laser scanning confocal microscopy.

To distinguish live and dead yeast, the LIVE/DEAD yeast viability kit (ThermoFisher Scientific, UK) was employed. This kit combines a two-color fluorescent assay, FUN™ 1 (green), with fluorescent fungal surface labeling reagent and Calcofluor White M2R (blue) that marks cell wall chitin with blue fluorescence independent of metabolic state. Only when the membrane integrity of fungi is maintained can the green fluorescence intracellular stain of FUN™ 1 be seen. This results in intracellular green labeling with blue envelope labeling of living cells and non-labeling when the yeast cells are disrupted. The yeast cells were stained by adding 1 mL of component A (FUN™ 1 cell stain) and 5 mL of Component B (Calcofluor White M2R) to 1 mL of yeast suspension. The mixture was incubated at 30 °C in the dark for 30 min. Finally, 10 μL of the stained cells were dropped on poly-L-lysine-covered slides and sealed with a coverslip. Slides were visualized by laser scanning confocal microscopy.

2.10. Statistical analysis

Data were statistically processed using Statgraphics Centurion XVIII (Statpoint Technologies, Inc., Warrenton, VA, USA). The differences observed between the amount of Cin released according to time and the differences in microbial viability according to treatments were analyzed by the Student's *t*-test for paired samples. The influence of the different treatment formulations (free Cin or the nanodevice **$MSN_{EPL\text{-}Cin}$**) and treatment concentrations for MIC, MBC, MFC and microbial viability determination by fluorescent viability staining assays were analyzed by an analysis of variance (multifactorial ANOVA). The LSD (least significant difference) procedure was used to test differences between averages at the 5 % significance level.

3. Results and discussion

3.1. Design, synthesis, and characterization of gated nanodevice

The designed smart antimicrobial nanodevice **$MSN_{EPL\text{-}Cin}$** contains three different elements: (i) MSNs as inorganic support, (ii) cinnamaldehyde as naturally occurring antimicrobial, and (iii) the polypeptide, ε-poly-L-lysine (EPL), which acts as a gatekeeper. MSNs were selected because of their high loading capacity and high surface area, which allows effective anchoring of organic molecules on the nanoparticle's surface. The EOC cinnamaldehyde was chosen for its antimicrobial properties and because it is Generally Recognized as Safe (GRAS) by the FDA [48]. Despite its excellent antimicrobial properties, cinnamaldehyde presents several disadvantages, such as high volatility, poor solubility, strong odor, and easy degradation. On the other hand, the molecular gate was selected due to the biocompatibility of the polypeptide, ε-poly-L-lysine (EPL), which can be degraded with proteases. As a result of the combination of these three elements, the nanodevice **$MSN_{EPL\text{-}Cin}$** was obtained. The preparation of the materials was carried out in four consecutive stages (Fig. 1): (i) synthesis of mesoporous support (**MSN_{cal}**), (ii) loading of cinnamaldehyde on the nanoparticles (**MSN_{Cin}**), (iii) functionalization of MSN with isocyanate groups (**$MSN_{NCO\text{-}Cin}$**) and (iv) coating with EPL (**$MSN_{EPL\text{-}Cin}$**).

As can be seen in Fig. 1, the synthetic route chosen to anchor the EPL molecular gate on the surface of the MCM-41-type nanoparticle was based on a carbamoylation, the formation of a urea bond between the attached isocyanate and the amine groups of EPL [35,36]. **MSN_{EPL}** (a solid capped with EPL without cinnamaldehyde) was also synthesized and used as a control.

The synthesized nanomaterials were characterized by standard techniques, as seen in Fig. 2. TEM images of the **MSN_{cal}** show the typical matrix of the MCM-41 material, composed of narrow channels with a hexagonal arrangement, and in the case of **$MSN_{EPL\text{-}Cin}$**, The presence of occluded organic matter inside the pores and on the surface of the nanoparticles confers a significant opacity to the nanoparticles and, due to the loss of contrast, the channels present in the initial scaffold are no longer clearly visible. However, it is observed that the loading and functionalization processes do not produce a considerable variation in the three-dimensional structure of the nanoparticles (Fig. 2A). The N_2

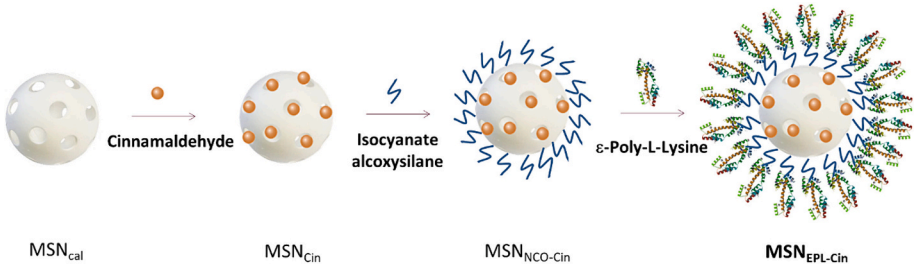

Fig. 1. Schematic representation of the synthetic route of **MSN$_{EPL-Cin}$**. Cargo loading was followed by isocyanate groups surface functionalization and lastly, the anchoring of EPL forming a urea bond between amine groups of EPL and isocyanate groups of the functionalized nanoparticle.

adsorption-desorption isotherms of the **MSN$_{cal}$** and **MSN$_{EPL}$** are shown in Fig. 2B. The **MSN$_{cal}$** support presents a characteristic adsorption step at P/P_0 values between 0.25 and 0.4, corresponding to a type IV isotherm. The adsorption and desorption curves are coincident, indicating that the adsorption mechanism is fully reversible. Besides, the absence of a hysteresis loop in this interval and the narrow BJH pore distribution suggest the existence of uniform cylindrical mesopores. The N_2 adsorption-desorption isotherm of **MSN$_{EPL}$** solid shows a significant decrease in the N_2 volume adsorbed, typical of mesoporous systems with practically filled mesoporous, and the curve is completely flat when compared (at the same scale) with empty MSNs.

Table S1 displays BET specific values, pore volumes and pore sizes calculated from N_2 adsorption-desorption isotherms for both solids. Application of the BET model resulted in a value for the total specific surface of 1118 $m^2 \cdot g^{-1}$ for **MSN$_{cal}$**, whereas this value is 130 $m^2 \cdot g^{-1}$ for **MSN$_{EPL}$**. The BJH model was applied at $P/P_0 < 0.6$ (associated with adsorption within pores) to obtain pore size and total pore volume. Fig. 2C shows powder X-ray diffraction patterns at low angles ($1.5 < 2\theta < 7$) of the MSN before and after calcination and the final nanodevice. The **MSN$_{asmade}$** (A) exhibits low-angle reflection peaks characteristic of MCM-41-type mesoporous nanoparticles. The peaks were indexed from left to right as (1 0 0), (1 1 0), (2 0 0), and (2 1 0) Bragg reflections, respectively. For the **MSN$_{cal}$** (B), a displacement of the peaks to higher 2θ values was observed as the interplanar distance decreased due to the condensation of silanol groups during the calcination procedure. The low angle reflection (1 0 0) is preserved in the final **MSN$_{EPL-Cin}$** material, while other peaks cannot be observed due to loss of contrast because of the loading and functionalization process. TEM images of **MSN$_{EPL-Cin}$** at low magnification show a population of spherical nanoparticles with a quite monodisperse distribution size at an average value of 84 ± 12 nm ($N = 115$) (Fig. 2D). As particle size and size distribution are crucial factors for the application uses, we have also calculated the polydispersity index (PDI) from the standard deviation and the average value of the size distribution of the nanodevice **MSN$_{EPL-Cin}$** [49]. The obtained value of 0.02 (entirely below the reference value of 0.1) shows a remarkable monodispertion in the distribution size of the nanoparticles. TEM-EDX mapping of **MSN$_{EPL-Cin}$** shows the presence of Si and O (from the silica scaffold) and N (from urea and EPL) (Fig. 2E). Thermogravimetric analysis (TGA) and forced cinnamaldehyde extraction with hexane allowed us to calculate an organic matter content of 92.8 mg Cin$\cdot g^{-1}$ solid and 364.0 mg EPL$\cdot g^{-1}$ solid (Table S2).

The hydrodynamic size and zeta potential of different synthesis steps of nanoparticles were also used to follow the functionalization and loading process (Table S3). For ζ potential study (Table S3), **MSN$_{cal}$** shows a value of −27.10 mV due to the presence of silanol groups. After the Cin loading and functionalization with isocyanate trialkoxysilane, the corresponding solid (**MSN$_{NCO-Cin}$**) displays a less negative surface potential due to the condensation of silanol groups with isocyanate trialkoxysilane. Finally, **MSN$_{EPL-Cin}$** presents a more negative ζ potential value that can be attributed to the condensation between amines from EPL and the isocyanate groups to form urea bonds, which leaves carboxylates of the EPL exposed on the surface. The fact that ζ potential of the **MSN$_{EPL-Cin}$** particles was negative agrees with a reduction of amine groups on the nanoparticle's surface and can be responsible for the lack of EPL antimicrobial activity on the solid **MSN$_{EPL}$** (vide infra). Table S3 also shows how the hydrodynamic size changes from 153.50 nm for **MSN$_{cal}$** to 242.3 nm for the final **MSN$_{EPL-Cin}$** nanoparticles.

Furthermore, infrared spectroscopy was used to ensure the correct encapsulation of Cin inside the pores and the functionalization and anchoring processes of the gatekeeper (vide supra). FT-IR spectra of all the solids within the 4000–400 cm^{-1} wavelength range are shown in Fig. 2F. Solids present the characteristic bands of the silica matrix; the stretching of the Si—O—Si bonds above 1060 cm^{-1}, the bending of the Si—O bond around 790 cm^{-1}, and a rocking signal at 450 cm^{-1}, as well as bands related to vibrations of water molecules (3420 and 1620 cm^{-1}). Some additional changes related to the functionalization process can be observed in smaller bands. Thus, **MSN$_{NCO-Cin}$** shows the decrease of the band at 960 cm^{-1} assignable to the vibration of the silanol group when the NCO group was anchored to the surface. In addition, the appearance of bands around 1700 cm^{-1} in **MSN$_{Cin}$**, attributed to the carbonyl group in Cin, and bands around 770–730 cm^{-1}, corresponding to the substituted benzene in Cin, are also observed. Finally, as in **MSN$_{EPL-Cin}$**, a broad band was found above 3000 cm^{-1}, attributed to water molecules adsorbed on the EPL gatekeeper.

Finally, release assays were performed to confirm the mechanism of the polypeptide EPL as gatekeeper. To demonstrate the ability of EPL to regulate the Cin-payload delivery from **MSN$_{EPL-Cin}$**, the delivery of Cin by UV–visible spectroscopy at 280 nm (as specified in Section 2.9) was studied. The release of the cargo when no protease was present was lower than in the presence of protease (Fig. 2G). This assay indicated the modulation of the antimicrobial release according to the presence of proteolytic enzymes in the medium. In the presence of a microbial protease, **MSN$_{EPL-Cin}$** released a maximum amount of Cin of 28.13 mg$\cdot$mg solid^{-1}. This amount corresponds to around 30 % of the cargo content (92.83 mg$\cdot$mg solid^{-1}) according to the results obtained in Section 3.1 (Table S2). The uncapping mechanism of the molecular gate allows an improvement in the delivery of the cargo when the target stimulus is present (i.e., proteases). Exposure of the microorganisms to the developed nanodevice is expected to lead to a sustained release of Cin with subsequent microbial inhibition and elimination.

3.2. Antimicrobial properties of the nanodevice

To confirm the biocidal properties of **MSN$_{EPL-Cin}$**, different assays with *E. coli*, *S. aureus*, and *C. albicans* were carried out. The bactericidal and fungicidal activity were evaluated in the first step by incubating the microorganisms with **MSN$_{EPL-Cin}$** and free Cin (at equivalent Cin concentrations) in a buffered solution. The dose-response results are shown in Fig. 3. Free Cin could not kill *E. coli*, *S. aureus*, and *C. albicans* after 24 h of incubation in the concentration range tested. In contrast, the incubation of the bacterial or fungal strains with the nanodevice resulted in the reduction of the viable bacterial count with complete elimination of the strains.

MSN$_{EPL-Cin}$ eliminated a bacterial cell concentration of 10^5

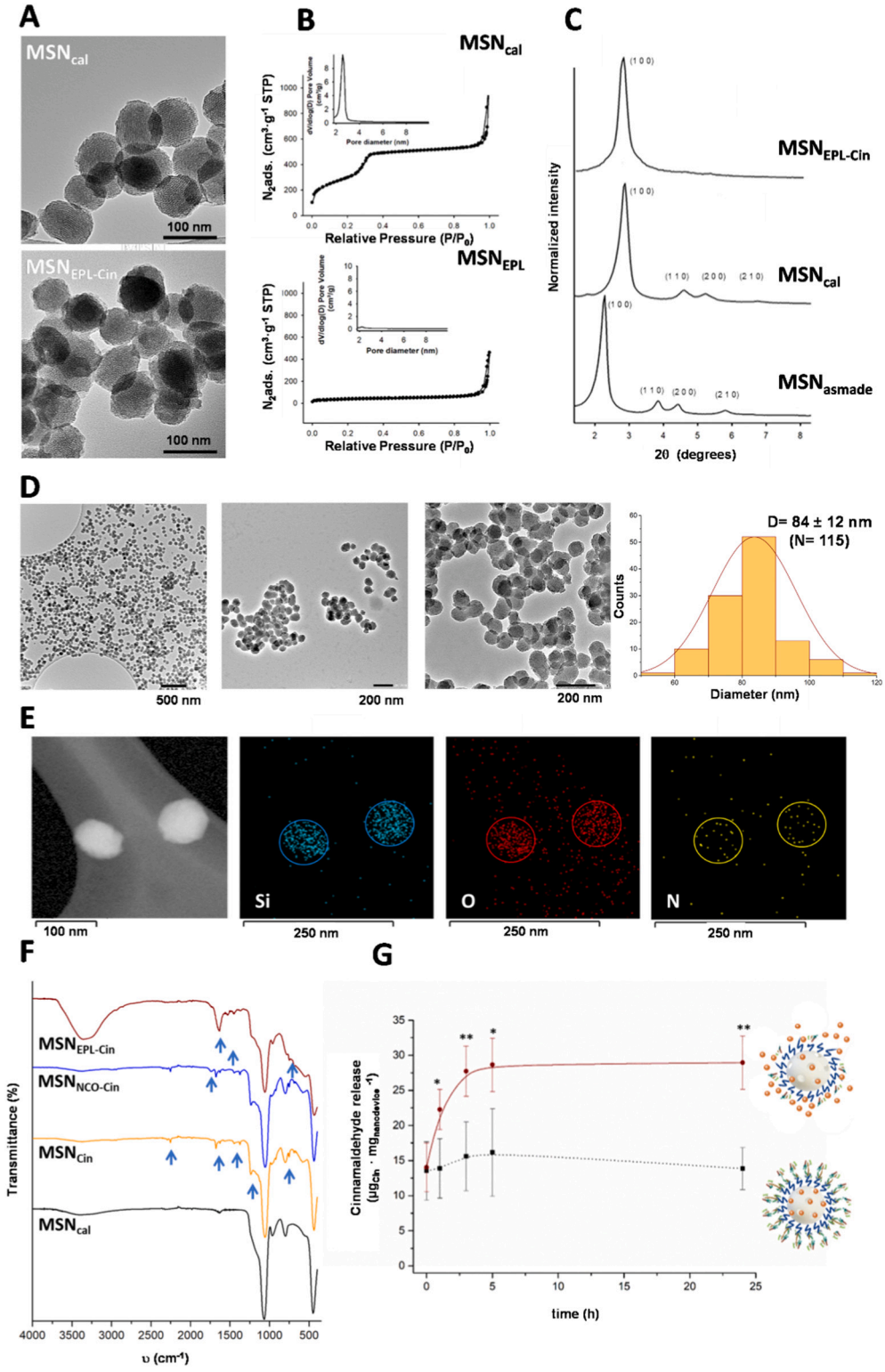

Fig. 2. Characterization of nanomaterials. TEM images (A) of the calcined mesoporous silica nanoparticles (**MSN_{cal}**) and **$MSN_{EPL\text{-}Cin}$**. N_2 adsorption-desorption isotherms (B) for **MSN_{cal}** and **MSN_{EPL}**. Normalized powder X-ray diffraction patterns (C) of the nanomaterials **MSN_{asmade}**, **MSN_{cal}**, and **$MSN_{EPL\text{-}Cin}$**. TEM images (D) of **$MSN_{EPL\text{-}Cin}$** and nanodevice size distribution graph obtained from analyzing the TEM images. TEM-EDX element mapping (E) of **$MSN_{EPL\text{-}Cin}$** showing the presence of Si and O (from the silica scaffold), and N (from NCO moieties and EPL molecular gate). FT-IR spectra (F) of **MSN_{cal}**, **MSN_{Cin}**, **$MSN_{NCO\text{-}Cin}$**, and **$MSN_{EPL\text{-}Cin}$**. Cinnamaldehyde release profile (G) from **$MSN_{EPL\text{-}Cin}$** in the absence (black curve, blank) and in the presence of protease (garnet curve, stimuli). Error bars correspond to the s.d. from three independent experiments. Data represent the mean ± SEM ($n \geq 3$), and statistical significance was assessed by the Student's *t*-test for paired samples ($^{*}p < 0.05$; $^{**}p < 0.01$; $^{***}p < 0.001$).

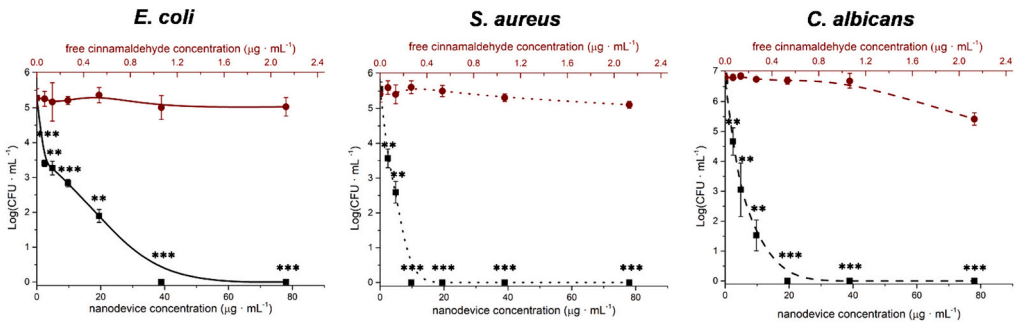

Fig. 3. Viability of *E. coli*, *S. aureus*, and *C. albicans* after 24 h of incubation in the presence of **MSN$_{EPL\text{-}Cin}$** (black) and equivalent concentrations of free cinnamaldehyde (garnet). Error bars correspond to the s.d. from three independent experiments. Data represent the mean ± SEM ($n \geq 3$), and statistical significance was assessed by the Student's *t*-test for paired samples (*$p < 0.05$; **$p < 0.01$; ***$p < 0.001$).

Table 1
Minimum inhibitory concentration (MIC) (μg of treatment per mL) and minimum bactericidal or fungicidal concentration (MBC or MFC) (μg of treatment per mL) values for **MSN$_{EPL\text{-}Cin}$** and free cinnamaldehyde (Cin) against different pathogenic microorganisms. Data represent the mean ($n \geq 9$), and statistical significance was assessed by the Student's *t*-test for paired samples (*$p < 0.05$; **$p < 0.01$; ***$p < 0.001$).

Microorganism	Treatment	MIC (μg·mL^{-1})	*P* value	MBC or MFC (μg·mL^{-1})	P value
E. coli	Cin	**333**	***	**500**	***
	MSN$_{EPL\text{-}Cin}$ (Cin$_{released}$)[a]	227 (**6.32**)		556 (**15.64**)	
S. aureus	Cin	**500**	***	**1000**	***
	MSN$_{EPL\text{-}Cin}$ (Cin$_{released}$)[a]	278 (**7.82**)		590 (**16.59**)	
C. albicans	Cin	**125**	***	**500**	***
	MSN$_{EPL\text{-}Cin}$ (Cin$_{released}$)[a]	1250 (**35.16**)		2500 (**70.33**)	

[a] MIC and MBC/MFC values of the nanodevice **MSN$_{EPL\text{-}Cin}$** are presented in μg of nanocarrier per mL. Values in brackets and in bold correspond to the amount of Cin free or the amount of Cin released by the nanodevice.

CFU·mL^{-1} of *E. coli* at the dose of 39.06 μg·mL^{-1} (1.099 μg·mL^{-1} of released Cin) and *S. aureus* at 9.77 μg·mL^{-1} (0.275 μg·mL^{-1} of released Cin). Moreover, the nanodevice was also highly effective in killing the yeast *C. albicans*. **MSN$_{EPL\text{-}Cin}$** killed a cell density of 10^7 CFU·mL^{-1} of *C. albicans* at the dose of 19.53 μg·mL^{-1} (0.549 μg·mL^{-1} Cin), whereas free Cin was able to decrease only one logarithmic cycle using a concentration of 2.19 μg·mL^{-1}.

The enhancement of the antimicrobial activity of the essential oil Cin is attributed to the decrease of its volatility when entrapped in the porous silica matrix and the increase of its local concentration due to the enhanced release in the presence of the pathogenic microorganisms. On the other hand, the antimicrobial activity of the unloaded **MSN$_{EPL}$** was also evaluated. Triplicate tests were performed in three independent assays against bacterial and yeast strains, showing no antibacterial or antifungal properties (data not shown). These results are consistent with previous data that reported that EPL loses its antimicrobial properties when its amine groups are hindered due to chemically functionalization and/or steric effects that may block the interaction of the EPL's amines with the microbial cell membrane [50].

As reported, EPL can undergo structural changes at different pH [51,52]. At pH below the pKa of the α-amino group, EPL was in an electrostatically extended conformation and, conversely, formed a β-sheet conformation. The antibacterial activity decreased slightly when the pH was higher than the isoelectric point (pI = 9). Under very low pH conditions, the antimicrobial activity of EPL remains at a level similar to alkaline conditions. The reason for this is the loss of counter-anionic charge of EPL, and structurally, a transformation from α-helical to random coil is observed [53]. When the chain amino group is modified by carbamoylation, it was determined that the conformation of EPL was affected by the pKa of the side chain amino group, and the secondary structure also changed to some β-sheet natures [50]. Considering this, **MSN$_{EPL}$** was tested in triplicate at different pH solutions, but no antimicrobial effects were found (data not shown).

This indicates that the activity of the nanodevice is due to the antimicrobial Cin, which is enhanced by its encapsulation inside the mesoporous silica nanocarrier and its enhanced delivery in the presence of proteases. Besides, the antibacterial and antifungal properties of **MSN$_{EPL\text{-}Cin}$** are remarkable compared to free Cin essential oil.

Once the antimicrobial properties of the nanodevice were established, the growth inhibitory activity of **MSN$_{EPL\text{-}Cin}$** was evaluated against microorganisms incubated in an optimal nutrient medium for their growth. Table 1 shows the growth inhibition capability in terms of MIC and MBC/MFC values of the nanodevice against *E. coli*, *S. aureus*, and *C. albicans* compared to free Cin. *E. coli* growth was inhibited by 227 μg·mL^{-1} of **MSN$_{EPL\text{-}Cin}$** (6.32 μg·mL^{-1} of released Cin) versus 333 μg·mL^{-1} of free cinnamaldehyde, enhancing the antimicrobial activity of Cin ca. 52-folds. In terms of MBC, 556 μg·mL^{-1} of **MSN$_{EPL\text{-}Cin}$**, corresponding to 15.64 μg·mL^{-1} of released Cin, were used to completely inhibit *E. coli*, whereas the MBC of free Cin was established at 500 μg·mL^{-1}, resulting in 32-fold higher antibacterial activity for the nanodevice. Statistical analysis confirms the significant differences between the inhibitory potential of antimicrobial treatments, as seen in Table 1.

In the case of *S. aureus*, **MSN$_{EPL\text{-}Cin}$** showed a MIC of 278 μg·mL^{-1} (7.82 μg·mL^{-1} of released Cin) versus 500 μg·mL^{-1} for free Cin. The MBC of the nanodevice was established at 590 μg·mL^{-1} of **MSN$_{EPL\text{-}Cin}$**, corresponding to 16.59 μg·mL^{-1} of released Cin, versus an MBC of 1000 μg·mL^{-1} for free Cin. Therefore, the inhibitory potential of the **MSN$_{EPL\text{-}Cin}$** for *S. aureus* was 60-fold higher than that of free Cin.

C. albicans growth was inhibited by 1250 μg·mL^{-1} of **MSN$_{EPL\text{-}Cin}$** (35.16 μg·mL^{-1} of released Cin) versus the MIC of free Cin established at 125 μg·mL^{-1}. In terms of MFC, the total inhibition of the yeast was achieved with 2500 μg·mL^{-1} of **MSN$_{EPL\text{-}Cin}$**, corresponding to 70.33 μg·mL^{-1} of released Cin, whereas the MBC of free Cin was established at 500 μg·mL^{-1}. These results showed a lesser but also remarkable extent of the inhibitory properties of the nanodevice for *C. albicans* with an improvement of 7-fold versus free Cin.

Regarding the results obtained for both MIC and MBC/MFC shown in

Table 1, it is observed that in the case of the free compound, the values obtained experimentally in our work are similar to those described in the literature [54–56]. On the other hand, we have also found in the literature other nanodevices that encapsulate natural bioactive compounds and are capped with a protein. However, they fall short of the efficacy of our **MSN$_{EPL-Cin}$** nanodevice. Specifically, mesoporous silica nanoparticles loaded with Cin and coated with the Zein protein were described by Poyatos-Rancionero et al. In this case, an MBC of 8 mg·mL^{-1} with a total Cin content of 113 μg·mL^{-1} against *E. coli* was reported [11]. Besides, Zein-capped MSNs and loaded the natural compounds capsaicin [57] and tea tree oil [58] have also been reported and tested against bacteria. In these works, the amount of nanoparticles required to reach the MBC was 1.5 mg·mL^{-1} against *S. aureus* and between 2 and 4 mg·mL^{-1} against *E. coli*, in the case of capsaicin and 0.6 mg·mL^{-1} against *S. aureus* and 1.2 mg·mL^{-1} against *E. coli* for tea tree oil. Comparing the use of these nanodevices with **MSN$_{EPL-Cin}$**, they are 2–4 times the amount of **MSN$_{EPL-Cin}$** needed to achieve similar results. Other similar systems were described against *S. aureus*, obtaining good results that cannot be compared with ours due to the different nature of the antimicrobial assays [59].

In addition, the viability of the free and encapsulated Cin-treated bacteria and yeast strains was determined by plate counting using two-color fluorescent dyes to visualize viable cells in terms of cell membrane integrity. Fig. 4 shows fluorescence images of the tested microbial strains treated with 1/2 MIC and MIC of **MSN$_{EPL-Cin}$**, and the equivalent concentration of free Cin, and a viable cells quantification for each treatment. Treatment conditions were selected based on the MIC results shown in Table 1.

As can be seen in Fig. 4, untreated bacteria strains (both *E. coli* and *S. aureus*) display fluorescence of the SYTO 9 fluorophore indicating that cells are viable. For untreated *C. albicans*, cells show intense green intracellular fluorescence due to the FUN™ 1 fluorophore and blue outline of Calcofluor White M2R stain that marks the chitin wall of viable yeast cells. There was a remarkable number of blastoconidia form cells and some pseudohyphae form cells in the sample due to the dimorphism of *C. albicans*. Treatment with free cinnamaldehyde resulted in no changes when compared with the untreated cells. However, when the cells were treated with 1/2 MIC of **MSN$_{EPL-Cin}$**, significant changes were already found. A clear decrease in the total cell number was observed for both bacteria and yeast. In addition, it was also observed an increase in the percentage of non-viable (marked in red) versus viable cells (Fig. 4). *S. aureus* and *E. coli* show a lower number of cells illuminated in green (viable) and a higher number of cells illuminated in red due to the propidium iodide fluorophore (non-viable). In the case of the yeast strain, fewer cells show an intense blue outline (viable cells) versus more cells with a light blue outline and green extracellular debris because of the nanodevice causing wall disruption and cell lysis (non-viable). Besides, when cells are treated with the amount of **MSN$_{EPL-Cin}$** corresponding to the MIC value, an even more drastic decrease in the number of cells per field, both viable and non-viable, was found. Under these conditions, many cells have been lysed, and a few red-stained cells are still detectable. In the *C. albicans* sample, only green debris due to cell lysis and the release of the intracellular matrix into the medium is visible. The ANOVA analysis showed significant differences ($p < 0.001$) between treatment with the nanodevice at different doses and the control (untreated) or treatment with free cinnamaldehyde. However, no significant differences were shown between these control and free cinnamaldehyde-treated microorganisms.

4. Conclusions

In this work, we developed mesoporous silica nanoparticles loaded with cinnamaldehyde and capped with ε-poly-L-lysine (**MSN$_{EPL-Cin}$**). Cargo is delivered through a bio-controlled uncapping mechanism due to the presence of exogenous proteolytic enzymes of the pathogenic microorganisms *E. coli*, *S. aureus*, and *C. albicans*. **MSN$_{EPL-Cin}$** shows excellent antimicrobial activity at very low doses, remarkably enhancing the inhibitory properties of cinnamaldehyde with a reduction of the biocidal dose of around 98 % in the case of bacterial strains and a decrease of 72 % for the yeast strain. **MSN$_{EPL-Cin}$** improves the antimicrobial efficacy of cinnamaldehyde when compared to the free compound, ca. 52-fold for *E. coli*, ca. 60-fold for *S. aureus*, and ca. 7-fold for *C. albicans*. The enhancement of the antimicrobial activity of the essential oil component is attributed to the decrease of its volatility due to its encapsulation in the porous silica matrix and the increase of its local concentration due to the selective and controlled release in the presence of the microorganisms. We believe that devices containing natural biocides (such as essential oil components) whose delivery is controlled by the presence of pathogens might find applications in fields such as biomedicine, food technology, agriculture, and many others.

CRediT authorship contribution statement

Ángela Morellá-Aucejo: Formal analysis, Investigation, Methodology, Writing – original draft. **Serena Medaglia:** Investigation, Methodology, Visualization. **María Ruiz-Rico:** Methodology, Supervision,

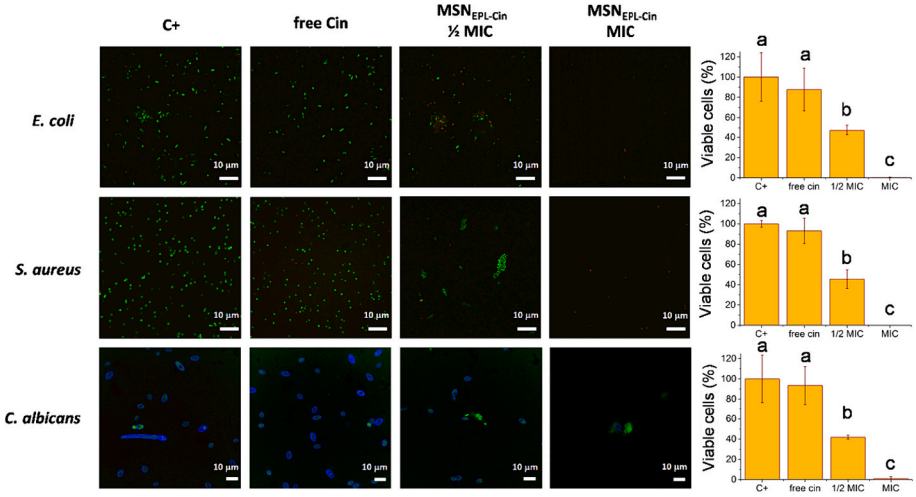

Fig. 4. Microbial viability determination by fluorescent viability staining. Fluorescence images and viable cells quantification of positive control (untreated microorganism), microorganisms treated with free Cin, 1/2 MIC of **MSN$_{EPL-Cin}$**, and MIC of **MSN$_{EPL-Cin}$** after 24 h of treatment. Mean values ($n = 3$) ± SD. Lower letters (a, b, c) indicate statistically significant differences among different treatments and concentrations ($p < 0.001$).

Writing – review & editing. **Ramón Martínez-Máñez:** Funding acquisition, Resources, Supervision, Writing – review & editing. **María Dolores Marcos:** Conceptualization, Funding acquisition, Project administration, Resources, Supervision, Writing – review & editing. **Andrea Bernardos:** Conceptualization, Funding acquisition, Project administration, Resources, Supervision, Writing – review & editing.

Declaration of competing interest

The authors declare that they have no known competing financial interests or personal relationships that could have appeared to influence the work reported in this paper.

Data availability

The raw/processed data required to reproduce these findings cannot be shared at this time due to technical or time limitations.

Acknowledgments

The authors thank the Electron Microscopy Service at UPV for their support.

Funding sources

This research was supported by projects PID2021-126304OB-C41 and PID2021-128141OB-C22 funded by MCIN/AEI/10.13039/501100011033/ and by European Regional Development Fund - A way of doing Europe. This study was also supported by Generalitat Valenciana (CIPROM/2021/007). This research was supported by CIBER -Consorcio Centro de Investigación Biomédica en Red- (CB06/01/2012), Instituto de Salud Carlos III, Ministerio de Ciencia e Innovación. This work was also funded by the Generalitat Valenciana and Agència Valenciana de la Innovación (MCIN) (INNEST/2021/169 project) and is susceptible to be co-founded by the European Union. Á. M.-A. thanks to the Universitat Politècnica de València (UPV) for her Ph. D. grant (DOCEMPR22). A.B. thanks the MCIN for her BG20/00020 contract and her PAID-PD-22 project funded by UPV.

Appendix A. Supplementary data

Supplementary data to this article can be found online at https://doi.org/10.1016/j.bioadv.2024.213840.

References

[1] M.E.A. de Kraker, A.J. Stewardson, S. Harbarth, Will 10 million people die a year due to antimicrobial resistance by 2050? PLoS Med. 13 (11) (Nov. 2016) e1002184 https://doi.org/10.1371/journal.pmed.1002184.

[2] I. Bergšpica, G. Kaprou, E.A. Alexa, M. Prieto-Maradona, A. Alvarez-Ordóñez, Identification of risk factors and hotspots of antibiotic resistance along the food chain using next-generation sequencing, EFSA J. (2020), https://doi.org/10.2903/j.efsa.2020.e181107.

[3] M. Hyldgaard, T. Mygind, R.L. Meyer, Essential oils in food preservation: mode of action, synergies, and interactions with food matrix components, Front. Microbiol. (2012), https://doi.org/10.3389/fmicb.2012.00012.

[4] H.A. Shaaban, Essential oil as antimicrobial agents: efficacy, stability, and safety issues for food application, in: Essential Oils - Bioactive Compounds, New Perspectives and Applications, IntechOpen, 2020.

[5] A.C. Stratakos, A. Koidis, Methods for extracting essential oils, in: Essential Oils in Food Preservation, Flavor and Safety, 2016.

[6] F. Nazzaro, F. Fratianni, L. De Martino, R. Coppola, V. De Feo, Effect of essential oils on pathogenic bacteria, Pharmaceuticals 6 (12) (Nov. 2013) 1451–1474, https://doi.org/10.3390/ph6121451.

[7] P.S.X. Yap, B.C. Yiap, H.C. Ping, S.H.E. Lim, Essential oils, a new horizon in combating bacterial antibiotic resistance, Open Microbiol. J. 8 (1) (Feb. 2014) 6–14, https://doi.org/10.2174/1874285801408010006.

[8] F.J. Álvarez-Martínez, E. Barrajón-Catalán, V. Micol, Tackling antibiotic resistance with compounds of natural origin: a comprehensive review, Biomedicines 8 (10) (Oct. 2020) 405, https://doi.org/10.3390/biomedicines8100405.

[9] A.A. Doyle, J.C. Stephens, A review of cinnamaldehyde and its derivatives as antibacterial agents, Fitoterapia 139 (Nov. 2019) 104405, https://doi.org/10.1016/j.fitote.2019.104405.

[10] K. Laird, C. Phillips, Vapour phase: a potential future use for essential oils as antimicrobials? Lett. Appl. Microbiol. 54 (3) (Mar. 2012) 169–174, https://doi.org/10.1111/j.1472-765X.2011.03190.x.

[11] E. Poyatos-Racionero, et al., Towards the enhancement of essential oil components' antimicrobial activity using new zein protein-gated mesoporous silica microdevices, Int. J. Mol. Sci. 22 (2021) 3795, vol. 22, no. 7, p. 3795, Apr. 2021, https://doi.org/10.3390/IJMS22073795.

[12] A. García-Fernández, et al., 902242 (1 of 62) New Advances in In Vivo Applications of Gated Mesoporous Silica as Drug Delivery Nanocarriers, 2019, https://doi.org/10.1002/smll.201 902242.

[13] M. Ruiz-Rico, É. Pérez-Esteve, J.M. Barat, Use of nanotechnology as an antimicrobial tool in the food sector, in: Nanobiotechnology, Taylor & Francis, Boca Raton, 2018, pp. 413–452. CRC Press, 2018.

[14] M. Ding, et al., Molecular manipulation of the microenvironment of au active sites on mesoporous silica for the enhanced catalytic reduction of 4-nitrophenol, Cat. Sci. Technol. (2023), https://doi.org/10.1039/D2CY02023H.

[15] E. Aznar, M. Oroval, L. Pascual, J.R. Murguía, R. Martínez-Máñez, F. Sancenón, Gated materials for on-command release of guest molecules, Chem. Rev. 116 (2) (Jan. 2016) 561–718, https://doi.org/10.1021/acs.chemrev.5b00456.

[16] A. García-Fernández, F. Sancenón, R. Martínez-Máñez, Mesoporous silica nanoparticles for pulmonary drug delivery, Adv. Drug Deliv. Rev. 177 (Oct. 2021) 113953, https://doi.org/10.1016/J.ADDR.2021.113953.

[17] A. Bernardos, et al., Antifungal effect of essential oil components against Aspergillus niger when loaded into silica mesoporous supports, J. Sci. Food Agric. 95 (14) (Nov. 2015) 2824–2831, https://doi.org/10.1002/jsfa.7022.

[18] A. Frankova, et al., The antifungal activity of essential oils in combination with warm air flow against postharvest phytopathogenic fungi in apples, Food Control 68 (Oct. 2016) 62–68, https://doi.org/10.1016/j.foodcont.2016.03.024.

[19] M. Ruiz-Rico, É. Pérez-Esteve, M.J. Lerma-García, M.D. Marcos, R. Martínez-Máñez, J.M. Barat, Protection of folic acid through encapsulation in mesoporous silica particles included in fruit juices, Food Chem. 218 (Mar. 2017) 471–478, https://doi.org/10.1016/J.FOODCHEM.2016.09.097.

[20] A. Estepa-Fernández, et al., Senolysis reduces senescence in veins and Cancer cell migration, Adv. Ther. (Aug. 2021) 2100149, https://doi.org/10.1002/adtp.202100149.

[21] A. Lérida-Viso, et al., Pharmacological senolysis reduces doxorubicin-induced cardiotoxicity and improves cardiac function in mice, Pharmacol. Res. 183 (Sep. 2022), https://doi.org/10.1016/J.PHRS.2022.106356.

[22] L. Pla, M.C. Martínez-Bisbal, E. Aznar, F. Sancenón, R. Martínez-Máñez, S. Santiago-Felipe, A fluorogenic capped mesoporous aptasensor for gluten detection, Anal. Chim. Acta 1147 (Feb. 2021) 178–186, https://doi.org/10.1016/j.aca.2020.12.060.

[23] E. Garrido, et al., Strip-based lateral flow-type indicator displacement assay for γ-hydroxybutyric acid (GHB) detection in beverages, Sens. Actuators B 377 (Feb. 2023), https://doi.org/10.1016/J.SNB.2022.133043.

[24] B. de Luis, et al., A chemical circular communication network at the nanoscale, Chem. Sci. (2021), https://doi.org/10.1039/d0sc04743k.

[25] B. de Luis, et al., Nanoprogrammed cross-kingdom communication between living microorganisms, Nano Lett. 22 (5) (Mar. 2022) 1836–1844, https://doi.org/10.1021/ACS.NANOLETT.1C02435.

[26] M. Martínez-Carmona, I. Izquierdo-Barba, M. Colilla, M. Vallet-Regí, Concanavalin A-targeted mesoporous silica nanoparticles for infection treatment, Acta Biomater. 96 (2019) 547–556, https://doi.org/10.1016/j.actbio.2019.07.001.

[27] M. Martínez-Carmona, D. Lozano, M. Colilla, M. Vallet-Regí, Lectin-conjugated pH-responsive mesoporous silica nanoparticles for targeted bone cancer treatment, Acta Biomater. 65 (2018) 393–404, https://doi.org/10.1016/j.actbio.2017.11.007.

[28] É. Pérez-Esteve, et al., Encapsulation of folic acid in different silica porous supports: a comparative study, Food Chem. 196 (Apr. 2016) 66–75, https://doi.org/10.1016/j.food-chem.2015.09.017.

[29] D. Muñoz-Espín, et al., A versatile drug delivery system targeting senescent cells, EMBO Mol. Med. 10 (9) (2018) 1–18, https://doi.org/10.15252/emmm.201809355.

[30] A. Estepa-Fernández, et al., Engineering nanoparticle communication in living systems by stigmergy: an application to enhance antitumor therapy in triple-negative breast cancer, Nano Today 48 (Feb. 2023) 101692, https://doi.org/10.1016/j.nantod.2022.101692.

[31] N. Mas, et al., Towards the development of smart 3D 'gated scaffolds' for on-command delivery, Small 10 (23) (Dec. 2014) 4859–4864, https://doi.org/10.1002/smll.201401 227.

[32] B. Rodrigues, et al., Antimicrobial activity of epsilon-poly-l-lysine against phytopathogenic bacteria, Sci. Rep. (2020), https://doi.org/10.1038/s41598-020-68262-1.

[33] T. Yoshida, T. Nagasawa, Poly-l-lysine: microbial production, biodegradation and application potential, Appl. Microbiol. Biotechnol. 62 (1) (Jul. 2003) 21–26, https://doi.org/10.1007/s00253-003-1312-9.

[34] I. Shih, M. Shen, Y. Van, Microbial synthesis of poly(ε-lysine) and its various applications, Bioresour. Technol. 97 (9) (Jun. 2006) 1148–1159, https://doi.org/10.1016/j.biortech.2004.08.012.

[35] A. García-Fernández, et al., Targeting inflammasome by the inhibition of caspase-1 activity using capped mesoporous silica nanoparticles, J. Control. Release 248 (Feb. 2017) 60–70, https://doi.org/10.1016/J.JCONREL.2017.01.002.

[36] C. de la Torre, et al., ϵ-polylysine-capped mesoporous silica nanoparticles as carrier of the C 9 h peptide to induce apoptosis in cancer cells, Chem. A Eur. J. 24 (8) (Feb. 2018) 1890–1897, https://doi.org/10.1002/chem.201704161.
[37] Y. Song, et al., Epsilon-poly-l-lysine decorated ordered mesoporous silica contributes to the synergistic antifungal effect and enhanced solubility of a lipophilic drug, Mater. Sci. Eng. C 99 (Jun. 2019) 231–240, https://doi.org/10.1016/J.MSEC.2019.01.077.
[38] L. Cai, et al., Schiff-base silver nanocomplexes formation on natural biopolymer coated mesoporous silica contributed to the improved curative effect on infectious microbes, Nano Res. 14 (8) (Aug. 2021) 2735–2748, https://doi.org/10.1007/S12274-020-3279-6/METRICS.
[39] C. Wandersman, Secretion, processing and activation of bacterial extracellular proteases, Mol. Microbiol. 3 (12) (1989) 1825–1831, https://doi.org/10.1111/j.1365-2958.1989.tb00169.x.
[40] L.M. Panicker, R. Usha, S. Roy, C. Mandal, Purification and characterization of a serine protease (CESP) from mature coconut endosperm, BMC. Res. Notes 2 (1) (2009) 81, https://doi.org/10.1186/1756-0500-2-81.
[41] L.P. Wackett, Microbial enzyme secretion, J. Microbial. Biotechnol. 10 (2) (Mar. 2017) 513–514, https://doi.org/10.1111/1751-7915.12702.
[42] A. Brandelli, The interaction of nanostructured antimicrobials with biological systems: cellular uptake, trafficking and potential toxicity, Food Sci. Human Wellness 9 (1) (Mar. 2020) 8–20, https://doi.org/10.1016/j.fshw.2019.12.003.
[43] D.R. Boettner, R.J. Chi, S.K. Lemmon, Lessons from yeast for clathrin-mediated endocytosis, Nat. Cell Biol. 14 (1) (Jan. 2012) 2–10, https://doi.org/10.1038/ncb2403.
[44] A.A. Miles, S.S. Misra, J.O. Irwin, The estimation of the bactericidal power of the blood, Epidemiol. Infect. 38 (6) (Nov. 1938) 732–749, https://doi.org/10.1017/S002217240001158X.
[45] CLSA, Methods for Dilution Antimicrobial Susceptibility Tests for Bacteria That Grow Aerobically; Approved Standard — Ninth Edition vol. 32, 2012 no. 2.
[46] J.H. Rex, et al., Reference method for broth dilution antifungal susceptibility testing of yeasts: approved standard - third edition 28 (April) (2008).
[47] M. Elshikh, et al., Resazurin-based 96-well plate microdilution method for the deter- mination of minimum inhibitory concentration of biosurfactants, Biotechnol. Lett. 38 (6) (Jun. 2016) 1015–1019, https://doi.org/10.1007/s10529-016-2079-2.
[48] S. Burt, Essential oils: their antibacterial properties and potential applications in foods—a review, Int. J. Food Microbiol. 94 (3) (Aug. 2004) 223–253, https://doi.org/10.1016/j.ijfoodmicro.2004.03.022.
[49] K.N. Clayton, J.W. Salameh, S.T. Wereley, T.L. Kinzer-Ursem, Physical characterization of nanoparticle size and surface modification using particle scattering diffusometry, Biomicrofluidics 10 (5) (Sep. 2016), https://doi.org/10.1063/1.4962992/133989.
[50] J.-N. Liu, et al., Structural changes and antibacterial activity of epsilon-poly-<scp>l</scp> -lysine in response to pH and phase transition and their mechanisms, J. Agric. Food Chem. 68 (4) (Jan. 2020) 1101–1109, https://doi.org/10.1021/acs.jafc. 9b07524.
[51] A. Mirtič, J. Grdadolnik, The structure of poly-l-lysine in different solvents, Biophys. Chem. 175–176 (May 2013) 47–53, https://doi.org/10.1016/J.BPC.2013.02.004.
[52] M.K. Kokufuta, S. Sato, E. Kokufuta, Swelling–shrinking behavior of chemically cross-linked polypeptide gels from poly(α-l-lysine), poly(α-dl-lysine), poly(ε-l-lysine) and thermally prepared poly(lysine): effects of pH, temperature and additives in the solution, Colloids Surf. B Biointerfaces 87 (2) (Oct. 2011) 299–309, https://doi.org/10.1016/J.COLSURFB.2011.05.033.
[53] M.M. Tomczak, et al., Polypeptide-templated synthesis of hexagonal silica platelets, J. Am. Chem. Soc. 127 (36) (Sep. 2005) 12577–12582, https://doi.org/10.1021/JA0524503/SUPPL_FILE/JA0524503SI20050715_021718.PDF.
[54] L. Ying, et al., The inhibition of trans-cinnamaldehyde on the virulence of Candida albicans via enhancing farnesol secretion with low potential for the development of resistance, Biochem. Biophys. Res. Commun. 515 (4) (Aug. 2019) 544–550, https://doi.org/10.1016/J.BBRC.2019.05.165.
[55] T.A.F. Ferro, et al., Cinnamaldehyde inhibits Staphylococcus aureus virulence factors and protects against infection in a galleria mellonella model, Front. Microbiol. 7 (DEC) (Dec. 2016) 1–10, https://doi.org/10.3389/fmicb.2016.02052.
[56] S. Shen, T. Zhang, Y. Yuan, S. Lin, J. Xu, H. Ye, Effects of cinnamaldehyde on Escherichia coli and Staphylococcus aureus membrane, Food Control 47 (Jan. 2015) 196–202, https://doi.org/10.1016/j.foodcont.2014.07.003.
[57] H. Sun, Y. Lu, J. Sheng, Y. Song, Zein-functionalized MCM-41 silica nanoparticles with enzyme-responsive for controlled release in antibacterial activity, Coatings 13 (1) (2023), https://doi.org/10.3390/coatings13010057.
[58] X. Zhong, F. Gao, H. Wei, H. Zhou, X. Zhou, Functionalization of mesoporous silica as an effective composite carrier for essential oils with improved sustained release behavior and long-term antibacterial performance, Nanotechnology 33 (3) (2022), https://doi.org/10.1088/1361-6528/ac2fe2.
[59] X. Liu, et al., Zein/MCM-41 nanocomposite film incorporated with cinnamon essential oil loaded by modified supercritical CO2 impregnation for long-term antibacterial packaging, Pharmaceutics 12 (2) (2020), https://doi.org/10.3390/pharmaceutics12020169.